Editors' Suggestion

Valence and magnetism in $EuPd_3S_4$ and $(Y, La)_xEu_{1-x}Pd_3S_4$

D. H. Ryan
Physics Department and Centre for the Physics of Materials, McGill University, 3600 University Street, Montreal, Quebec H3A 2T8, Canada

Sergey L. Bud'ko, Brinda Kuthanazhi, and Paul C. Canfield
Ames National Laboratory, and Department of Physics and Astronomy, Iowa State University, Ames, Iowa 50011, USA

(Received 7 October 2022; accepted 13 December 2022; published 5 January 2023)

^{151}Eu Mössbauer spectroscopy shows that yttrium substitution in mixed-valent $EuPd_3S_4$ drives the initial 50:50 mix of Eu^{3+} and Eu^{2+} towards pure Eu^{2+}, whereas lanthanum substitution has the opposite effect, but only for substitution levels above 50%. We find that total valence electron count and chemical pressure effects cannot account for the observed behavior; however, conserving the cell volume provides a consistent description of the changes in the Eu^{2+} : Eu^{3+} ratio. Remarkably, lanthanum substitution also leads to a clear transition from static mixed-valent behavior at lower temperatures to dynamic mixed-valent behavior at higher temperatures, with the onset temperature monotonically increasing with Eu content and extrapolating to a value of ∼340 K for the pure $EuPd_3S_4$ compound. Magnetic order persists at least as far as $x = 0.875$ in both series, despite the drastic reduction in the amount of moment-carrying Eu^{2+} ions.

DOI: 10.1103/PhysRevB.107.014402

I. INTRODUCTION

The rare-earth palladium sulfides RPd_3S_4 have been reported for the majority of the rare earths, including yttrium [1–4]. They all crystallize in the cubic $NaPt_3O_4$ structure ($Pm\bar{3}n$, No. 223) with the rare earth occupying the 2*a* site forming a bcc sublattice, the palladium on the 6*d* site, and the sulphur on the 8*e* site. The structure is shown in Fig. 18 (in the Appendix). Remarkably, although the RPd_3S_4 phases exist for the trivalent rare earths, but apparently not for the divalent alkaline earths (Ca and Sr), when prepared with europium [5] or ytterbium [4] a roughly 50:50 mix of divalent and trivalent rare earth is found.

Here we will use chemical substitution of yttrium and lanthanum for europium to investigate the stability of the valence distribution and its effects on magnetic ordering. Although both ^{170}Yb and ^{151}Eu Mössbauer spectroscopy can generally be used to identify the valence of their respective target ions, for ^{170}Yb Mössbauer spectroscopy, the isomer shift between the two valence states is extremely small so the technique is almost totally dependent on the presence of an electric field gradient (EFG) at the Yb^{3+} ions to identify trivalent ytterbium. Unfortunately, the high symmetry of the 2*a* site makes the EFG contribution effectively zero and the presence of the Yb^{3+} ions is only apparent in the magnetically ordered state well below $T_N \sim 2$ K [4]. We will therefore only study $EuPd_3S_4$ using ^{151}Eu Mössbauer spectroscopy where the two valence states are clearly isolated by a large difference in isomer shift, even at ambient temperatures.

We find that by substituting Y for Eu, the remaining Eu sites become more and more divalent. In contrast, by substituting La for Eu, we find that initially, the remaining Eu sites stay roughly a 50:50 mixture of di- and trivalent Eu, but for higher La substitution levels, the remaining Eu rapidly becomes more trivalent. La substitution also leads to a transition from statically mixed-valent behavior at lower temperatures to dynamically mixed-valent behavior at higher temperatures with the onset temperature (T_{onset}) monotonically increasing with Eu content and passing through room temperature as pure $EuPd_3S_4$ is approached. Despite the decreasing fraction of moment-carrying Eu^{2+} ions, both $Y_xEu_{1-x}Pd_3S_4$ and $La_xEu_{1-x}Pd_3S_4$ continue to exhibit some form of magnetic order at least as far as $x = 0.875$, with transition temperatures of ∼3 K (Y) and ∼6 K (La).

II. EXPERIMENTAL METHODS

Polycrystalline samples of $EuPd_3S_4$ and $(Y, La)_xEu_{1-x}Pd_3S_4$ were prepared from stoichiometric mixtures of EuS (99.9%, American Elements), Y_2S_3 (99.9%), La_2S_3 (99%), Pd (99.95%), and S (99.5%), all from Alfa-Aesar. The powders were mixed and then pressed to form a dense pellet. This was loaded into an alumina crucible and sealed under a partial pressure of helium in a fused silica tube. The sample was heated to 650 °C over three hours, held for an hour, and then taken to 900 °C over a further three hours. After 75 hours at 900 °C, the sample was furnace cooled and removed once it reached ambient temperature. In most cases, this single thermal cycle was found to yield a single-phased product; however, when an impurity was found (typically PdS seen by x-ray diffraction or EuS seen in susceptibility vs temperature), the sample was crushed, pressed, and subjected to a second 75 hr annealing cycle to 900 °C to remove the impurity.

X-ray diffraction measurements were made on a Rigaku Miniflex-II diffractometer using a Cu-K_α source. The instrument calibration was checked using NIST 676a Al_2O_3 and

found to be consistent within fitted uncertainties. Full Rietveld refinement of the diffraction patterns was carried out using the GSAS/EXPGUI packages [6,7]. As all three species occupy special sites in the $Pm\bar{3}n$ structure, no positional parameters were adjusted during the fits. For the yttrium and lanthanum substituted samples, only random occupation of the Eu(2*a*) site was considered.

^{151}Eu Mössbauer spectroscopy measurements were carried out using a 4 GBq $^{151}SmF_3$ source, driven in sinusoidal mode. The drive motion was calibrated using a standard ^{57}Co$\underline{\text{Rh}}$/α-Fe foil. Isomer shifts are quoted relative to EuF_3 at ambient temperature. The 21.6 keV gamma rays were recorded using a thin NaI scintillation detector. For temperatures above 5 K, the samples were cooled in a vibration-isolated closed-cycle helium refrigerator with the sample in a helium exchange gas. Temperatures below 5 K were achieved using a helium flow cryostat while pumping on the sample space and using a needle valve to throttle the flow. The spectra were fitted to a sum of Lorentzian lines with the positions and intensities derived from a full solution to the nuclear Hamiltonian [8].

Temperature- and magnetic-field-dependent magnetization measurements ($1.8 \leqslant T \leqslant 300$ K, $0 \leqslant \mu_0 H \leqslant 7$ T) were performed using a Quantum Design MPMS-3 superconducting quantum interference device (SQUID) magnetometer. The sample was confined in a No. 4 gelatin capsule and a transparent drinking straw was used as a sample holder. Low-temperature heat-capacity measurements were made using a semiadiabatic thermal relaxation technique as implemented in the heat-capacity option of a Quantum Design Physical Property Measurement System (PPMS). For selected samples, the ^{3}He option was used to cool to ~0.4 K. Sintered samples of 20–70 mg mass with at least one flat surface were mounted on a microcalorimeter platform using Apiezon N grease. The addenda (platform + grease) heat capacity was measured separately for each sample and subtracted from the total heat capacity using the PPMS software. Although the samples possibly had reduced density, the measured sample coupling parameter took reasonable values of more than 97%.

III. RESULTS

A. $EuPd_3S_4$

Fitting the x-ray diffraction pattern of the $EuPd_3S_4$ sample showed it to be single phased with the expected cubic $NaPt_3O_4$ structure [2] and a lattice parameter of $a = 6.6786(1)$ Å (Fig. 1). The room-temperature ^{151}Eu Mössbauer spectrum showed two distinct contributions from Eu^{3+} and Eu^{2+} in the ratio 50.4(4):49.6(4), with the linewidth of the Eu^{2+} component being slightly broader, in complete agreement with previous reports [5]. On cooling to 5 K, the ratio becomes 46.2(5):53.8(5) (Fig. 2) as the Debye temperature of the Eu^{3+} component is slightly higher than that of the Eu^{2+} component. Fitting the temperature dependence of the two component areas to a simple Debye model, as shown in Fig. 3, yields Debye temperatures of 227(3) K (Eu^{3+}) and 204(3) K (Eu^{2+}). It is important to emphasize that any *apparent* changes in the Eu^{2+}:Eu^{3+} ratio with temperature in Fig. 3 do not reflect *actual* changes in the ratio, rather they are the result of the different temperature dependences of the recoil-free fractions

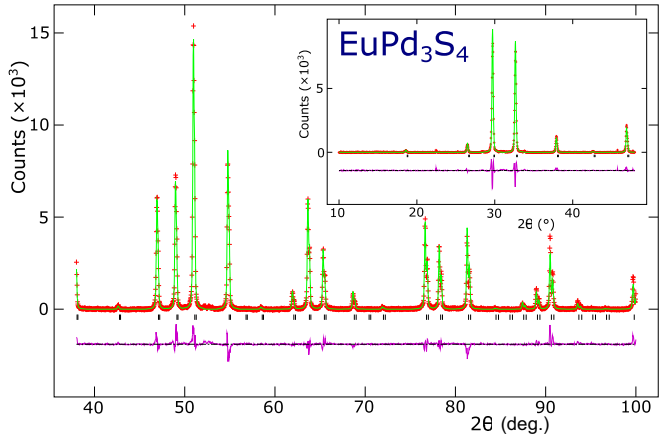

FIG. 1. Cu-K$_\alpha$ x-ray diffraction pattern for $EuPd_3S_4$. Solid line is a full Rietveld refinement using the GSAS/EXPGUI packages [6,7]. The line below the data shows the residuals. Tick marks between the data and residual lines show the calculated positions of the Bragg peaks. The inset shows the low-angle range. The diffraction pattern was collected in two overlapping blocks with a longer counting time at higher angles to compensate for the loss of intensity due to the effects of the x-ray form factor.

(often denoted *f*) for the two species. In order to minimize the impacts of this effect, all valence ratios will be taken from low-temperature spectra.

On cooling to 1.8 K, the Eu^{2+} component develops a clear magnetic splitting, whereas the Eu^{3+} component is unchanged, consistent with the trivalent europium being nonmagnetic (Fig. 2). In principle, one might anticipate a small transferred field at the Eu^{3+} sites from the ordered Eu^{2+} moments; however, none was observed and no increase in the width of the Eu^{3+} component was detected ($B_{hf} \ll 1$ T), perhaps as a result of cancellations arising from the antiferromagnetic ordering of the Eu^{2+} moments. The hyperfine field (B_{hf}) for the Eu^{2+} component at 1.8 K is 29.9(2) T, typical for ordered Eu^{2+}, and fitting the temperature dependence shown in Fig. 4 to the expected $J = \frac{7}{2}$ Brillouin function yields a $T = 0$, $B_{hf} = 37.9(6)$ T and an ordering temperature of $T_N = 2.90(1)$ K, in good agreement with both previous work [5] and our own susceptibility and C_p data (Fig. 5). The clear cusp in the susceptibility vs temperature is consistent with antiferromagnetic (AF) ordering and it is accompanied by a sharp peak in the heat capacity. The high-field magnetization curve taken at 1.8 K (inset to Fig. 5) shows that the system is readily saturated despite the AF order, consistent with the low ordering temperature as well as the low anisotropy typically associated with the Eu^{2+} ion. Furthermore, the maximum moment observed in the applied field of 7 T suggests a Eu^{2+} fraction of 50% (assuming a moment of 7 μ_B/Eu^{2+}), consistent with the 53.8(5)% derived above from the ^{151}Eu Mössbauer spectrum at 5 K, and with earlier results [5,9].

The unusual and apparently stable valence mix in $EuPd_3S_4$ leads to the following questions: "Why?" What makes europium (and ytterbium) "special"? How robust is the valence distribution? Can we change it?

As the Eu^{3+} ion is smaller than the Eu^{2+} ion, one might expect hydrostatic pressure to promote $Eu^{2+} \rightarrow Eu^{3+}$

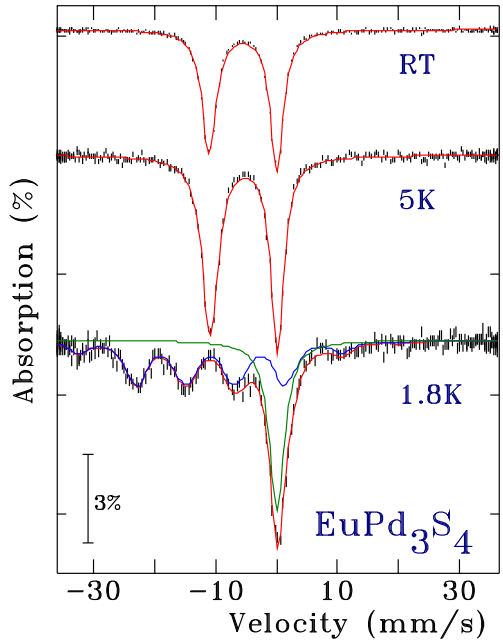

FIG. 2. ^{151}Eu Mössbauer spectra of $EuPd_3S_4$ at room temperature (RT) (top), 5 K (middle), and 1.8 K (bottom). Between RT and 5 K, the primary changes are a significant increase in the absorption due to conventional thermal effects and a slight change in the 2+:3+ area ratio due to differences in the Debye temperatures of the two components. At 5 K, the two valence contributions are almost equal in area and fully resolved, with the Eu^{2+} at −10.91(2) mm/s and Eu^{3+} at +0.07(1) mm/s. At 1.8 K, only the Eu^{2+} component is ordered and shows a hyperfine field (B_{hf}) of 29.9(2) T, while the Eu^{3+} component is unchanged. The solid red lines are fits as described in the text. For the 1.8 K spectrum, we also show the magnetically split Eu^{2+} and unchanged Eu^{3+} components.

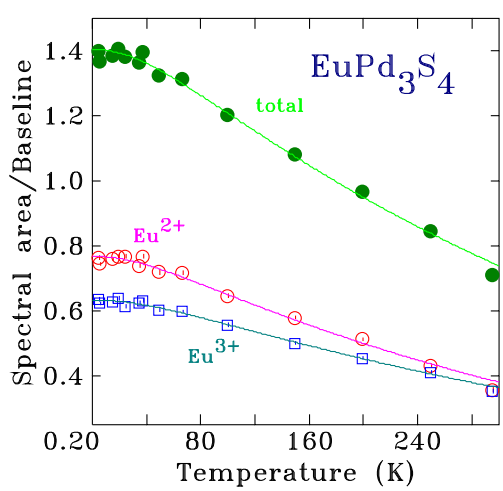

FIG. 3. Temperature dependence of the normalized (adjusted for total counting time) area of both the total spectrum and the two valence components in the ^{151}Eu Mössbauer spectra of $EuPd_3S_4$. Solid lines in each case are fits to a simple Debye model yielding Debye temperatures of 227(3) K (Eu^{3+}) and 204(3) K (Eu^{2+}). Fitting the total spectral area yields an average Debye temperature of 212(3) K.

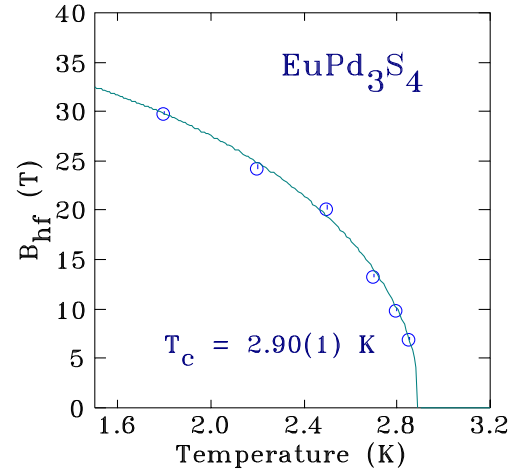

FIG. 4. Temperature dependence of hyperfine field (B_{hf}) for $EuPd_3S_4$ fitted using the expected $J = \frac{7}{2}$ Brillouin function to obtain the ordering temperature of $T_N = 2.90(1)$ K.

conversion. Alternatively, if we force some fraction of the R sites to be unambiguously trivalent, by replacing some of the europium with a formally trivalent ion, will this cause more of the remaining europium to become divalent to preserve the average electron count?

Although the driving that can be achieved by chemical substitution is not as clean as that generated by direct hydrostatic pressure, it is much easier to make direct measurements of

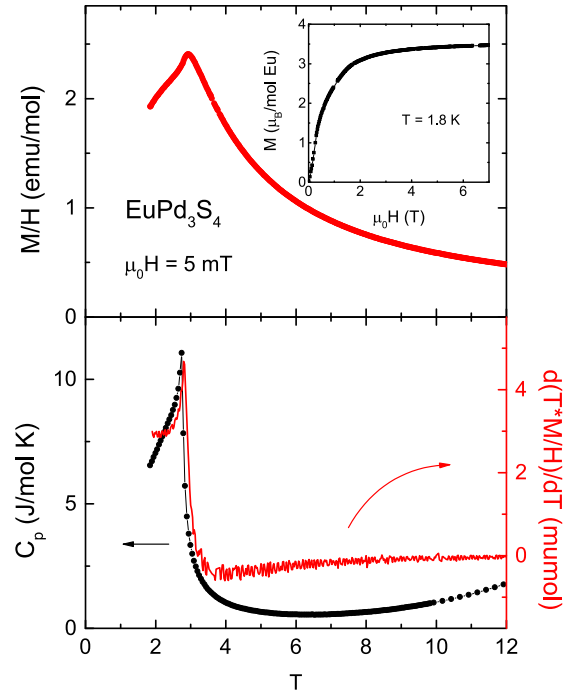

FIG. 5. Top: DC susceptibility vs temperature for $EuPd_3S_4$ showing a cusp at $T_N \sim 3$ K. Inset: M vs $\mu_0 H$ at 1.8 K, confirming that half of the europium is divalent. Bottom: Temperature dependence of the heat capacity (black points), revealing the corresponding cusp associated with the AF transition, with $d(T \cdot M/H)/dT$ (red line) showing that C_p (T) and the temperature derivative of $T \cdot M/H$ take the same form around the transition.

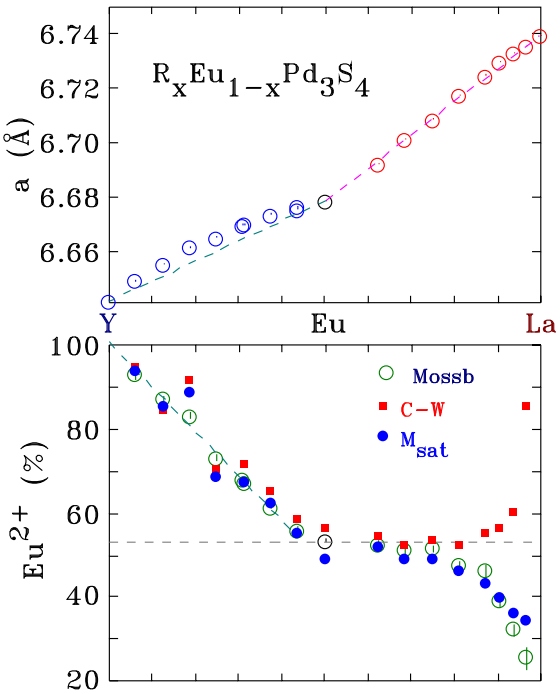

FIG. 6. Top: Lattice parameters for $(Y, La)_xEu_{1-x}Pd_3S_4$ showing the expansion associated with La substitution and the contraction when yttrium is substituted. We note that whereas the values for the La-substituted series lie on the line connecting the pure La and Eu compounds, those for the Y-substituted samples lie significantly above the corresponding line between the pure Eu and Y compounds. Bottom: The Eu^{2+} fractions in the pure and Y-,La-substituted compounds showing that Y substitution leads to a significant shift towards more Eu^{2+}, while La substitution initially appears to have no effect, but for $x > 0.5$ there is a marked shift towards Eu^{3+}. Open circles show values taken from ^{151}Eu Mössbauer spectroscopy at 5 K (Y substituted) or 10 K (La substituted). Solid symbols show values derived from bulk magnetization data: high-temperature Curie-Weiss fits (red squares) and saturation magnetization (blue circles). The deviation of the Curie-Weiss values for the La-rich compounds reflects the development of dynamic effects discussed in the text. Values used to construct this figure are given in Tables I and II in the Appendix.

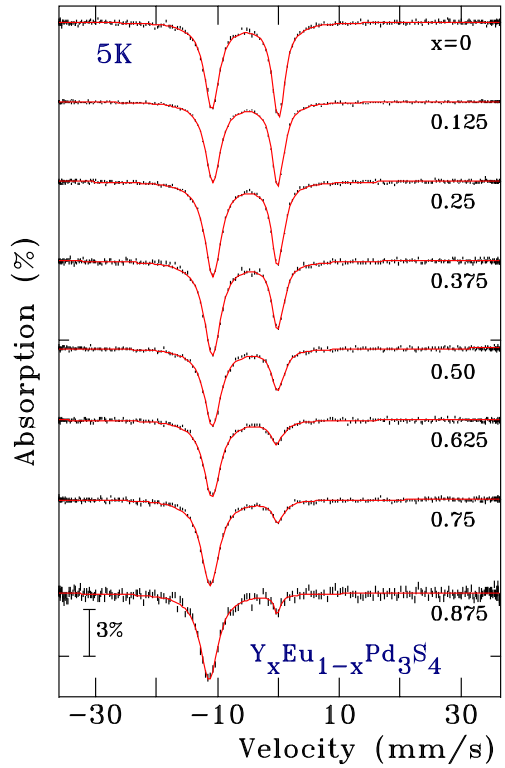

FIG. 7. ^{151}Eu Mössbauer spectra of $Y_xEu_{1-x}Pd_3S_4$ at 5 K showing the loss of the Eu^{3+} component (the line at ∼0 mm/s) as the level of yttrium substitution increases. The spectrum for $x = 0.875$ has been rescaled by a factor of 2.5 to compensate for the low Eu content.

the valence distribution, magnetization, and transition temperatures in doped samples at ambient pressures. We turn, therefore, to an investigation of the impacts of chemical substitution on $EuPd_3S_4$ using the non-moment-bearing, trivalent La and Y ions with $r_{\text{ionic}}(Eu^{2+}) \gtrsim r_{\text{ionic}}(La^{3+}) > r_{\text{ionic}}(Eu^{3+}) > r_{\text{ionic}}(Y^{3+})$. If, on the one hand, the total valence electron count is a dominant factor, then partially replacing the europium with an unambiguously trivalent ion should lead to a compensating increase in the Eu^{2+} fraction. On the other hand, if preserving the cell volume is critical, then the lattice expansion that would be caused by introducing the $r_{\text{ionic}}(La^{3+}) \lesssim r_{\text{ionic}}(Eu^{2+})$ lanthanum ion could be compensated by some $Eu^{2+} \rightarrow Eu^{3+}$ conversion [with the reverse expected for the $r_{\text{ionic}}(Y^{3+}) < r_{\text{ionic}}(Eu^{3+})$ yttrium ion]. Alternatively, if the substitutions act as chemical pressures, then expanding the cell using lanthanum substitution should lead to $Eu^{3+} \rightarrow Eu^{2+}$ conversion (again, the reverse process is expected for yttrium substitution). As we show below, we can clearly distinguish between these three options.

B. Valence impacts

Fitting the x-ray diffraction data for the yttrium- and lanthanum-substituted compounds showed that they all retained the expected $NaPt_3O_4$ structure, but with progressively smaller (Y) or larger (La) lattice parameters (Fig. 6). There is a clear, and significant, change in lattice parameters for both Y and La substitution. We detect no indication of phase separation in the powder x-ray diffraction data, i.e., no broadening or splitting of peaks that would suggest segregation of the samples into Eu-richer and Eu-poorer phases.

For the Y-substituted series, the fitted lattice parameters all lie visibly above the line connecting the Eu and Y compounds, suggesting that a shift towards more of the larger Eu^{2+} ion occurs as the yttrium content is increased. This valence shift is confirmed directly by the 5 K ^{151}Eu Mössbauer spectra shown in Fig. 7, where the line near 0 mm/s associated with the trivalent europium decreases rapidly in intensity as the level of yttrium substitution increases. (All valence ratios for the Y-substituted series were taken from 5 K spectra to minimize the impacts of *f*-factor differences for the two species, as noted above.) Both magnetization measurements in the ordered state at 1.8 K (Fig. 8) and Curie-Weiss fits to the temperature dependence of the susceptibility above 10 K further support these observations (see below). The Eu^{2+} fractions derived from all three measurements are summarized in the lower panel of Fig. 6.

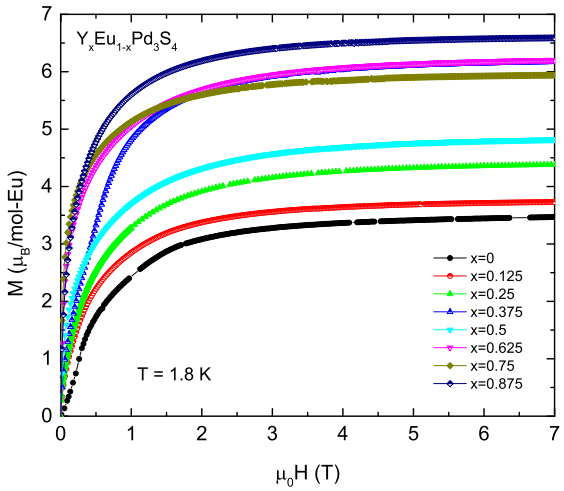

FIG. 8. High-field magnetization curves measured at 1.8 K for $Y_xEu_{1-x}Pd_3S_4$ showing the increase in moment/mol-Eu with increasing yttrium content as the substitution promotes $Eu^{3+} \rightarrow Eu^{2+}$ conversion. All of the curves appear to saturate in about 3–4 T, reflecting the low anisotropy associated with the Eu^{2+} ion.

By contrast with the yttrium-substituted series, the effects of lanthanum substitution are more complex and nuanced. The lattice parameters of the La-substituted compounds lie much closer to the line connecting the two end members (upper panel of Fig. 6) for all substitution levels, and the Eu^{2+} fraction derived from ^{151}Eu Mössbauer spectroscopy at 10 K (Fig. 9) is essentially constant (lower panel of Fig. 6) for $x \leqslant 0.5$. This is consistent with the fact that $r_{\text{ionic}}(Eu^{2+}) \gtrsim r_{\text{ionic}}(La^{3+}) > r_{\text{ionic}}(Eu^{3+})$ and initial La substitution does not force any significant change in the Eu^{2+}:Eu^{3+} ratio. However, once about half of the europium has been replaced by lanthanum, further substitution leads to a marked change in behavior, again consistent with the fact that $r_{\text{ionic}}(La^{3+})$ is ultimately somewhat closer to $r_{\text{ionic}}(Eu^{2+})$ rather than $r_{\text{ionic}}(Eu^{3+})$. It is readily apparent from Fig. 9 that the line near -11 mm/s that corresponds to Eu^{2+} decreases in relative intensity and this rapid loss of the divalent fraction is confirmed by the magnetization measurements shown in Fig. 10. We use 10 K Mössbauer data for the La-substituted series, rather than the 5 K data as was used for the Y-substituted series, to avoid complications due to the onset of magnetic ordering (see below).

Finally, as is clear in Fig. 6, the Eu^{2+} fraction derived from Curie-Weiss fits (data shown below) to the temperature dependence of the susceptibility, for $La_xEu_{1-x}Pd_3S_4$ with $x \gg 0.5$ (measured on the same sample as part of the run used to obtain the saturation magnetization), appears to show the *opposite* behavior—a marked *growth* in the effective moment and hence the derived Eu^{2+} fraction. As we show below, this is most likely due to dynamic effects that lead to intermediate-valence behavior of the europium ions and makes a simple Curie-Weiss analysis intractable over the temperature range available to us.

C. Dynamics in the yttrium and lanthanum substituted series

We have presented low-temperature Mössbauer data for the yttrium-substituted (5 K) and lanthanum-substituted (10 K)

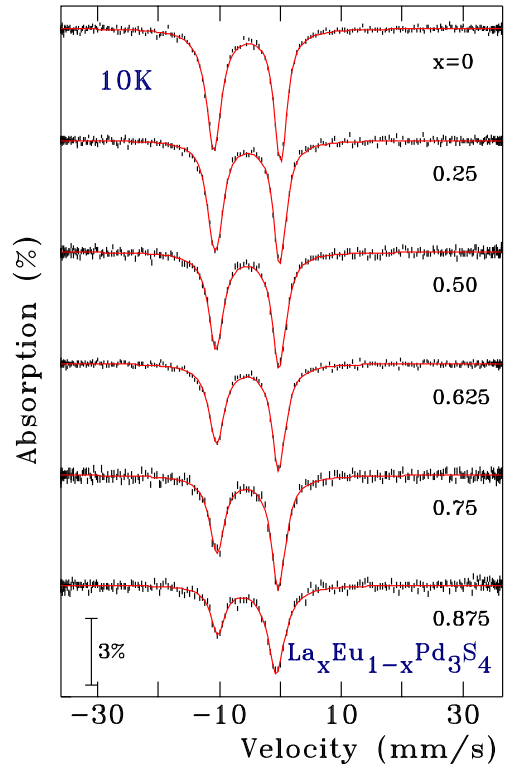

FIG. 9. ^{151}Eu Mössbauer spectra of $La_xEu_{1-x}Pd_3S_4$ at 10 K showing an essentially constant Eu^{2+}:Eu^{3+} distribution up to $x = 0.50$ followed by a marked drop in the Eu^{2+} fraction above that point. Spectra taken at 10 K are used here to avoid complications associated with the magnetic ordering of the Eu^{2+} component at 6 K.

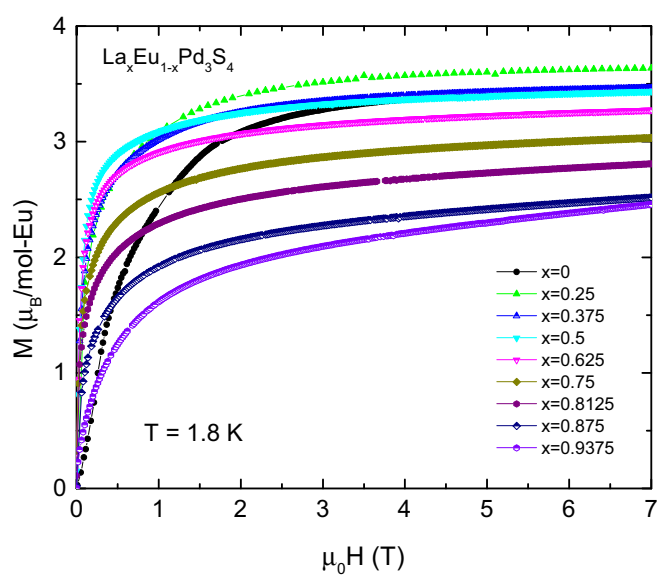

FIG. 10. High-field magnetization curves measured at 1.8 K for $La_xEu_{1-x}Pd_3S_4$ showing an approximately constant moment/mol-Eu with increasing lanthanum content up to $x = 0.5$ as the Eu^{2+}:Eu^{3+} ratio remains largely independent of the lanthanum content; then there is a marked drop as rapid $Eu^{2+} \rightarrow Eu^{3+}$ occurs.

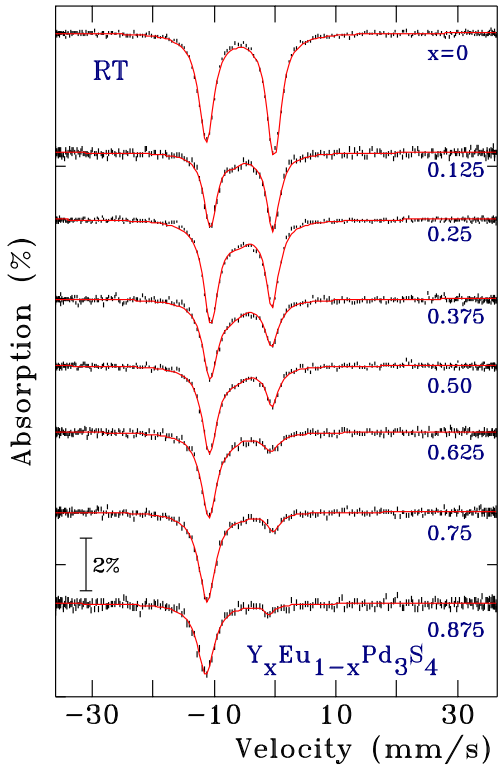

FIG. 11. Room-temperature ^{151}Eu Mössbauer spectra of $Y_xEu_{1-x}Pd_3S_4$ showing minimal changes from the 5 K spectra shown in Fig. 7 beyond the expected impacts of the differing Debye temperatures of the two valence components.

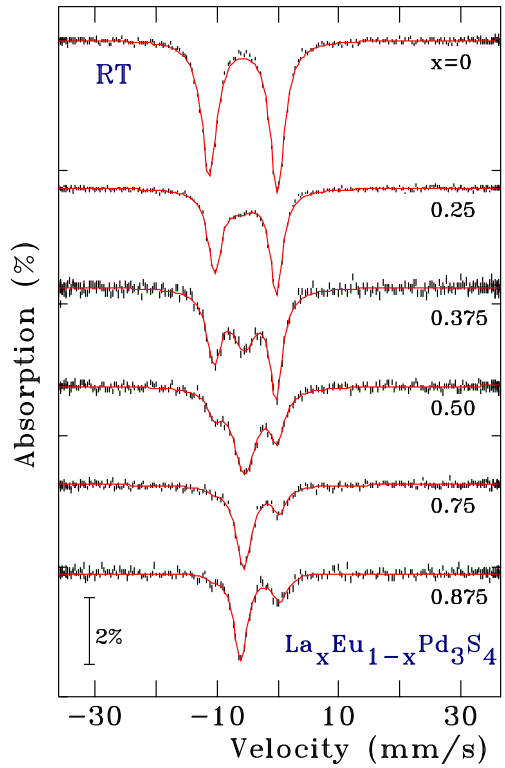

FIG. 12. Room-temperature ^{151}Eu Mössbauer spectra of $La_xEu_{1-x}Pd_3S_4$ showing the development of a new, intermediate-valence feature with increasing lanthanum content.

series in order to minimize the impacts of the differing Debye temperatures of the two valence components in the spectra. Figures 11 and 12 present the room-temperature Mössbauer spectra for the $Y_xEu_{1-x}Pd_3S_4$ and $La_xEu_{1-x}Pd_3S_4$ series. As can be seen, the differences between the room temperature and 5 K yttrium data are minimal and certainly not qualitative. However, for the $La_xEu_{1-x}Pd_3S_4$ series, the changes in the spectra on warming go far beyond the simple, and expected, slight reduction in the apparent Eu^{2+} fraction with increasing temperature. As is clear from the RT spectra of $La_xEu_{1-x}Pd_3S_4$ shown in Fig. 12, an entirely new feature appears in the spectra and eventually dominates the pattern by $x = 0.875$. This feature is a line located midway between the lines associated with Eu^{2+} and Eu^{3+}. As Fig. 13 shows, the position of this line is essentially composition independent, appearing for all compositions $0.25 \leqslant x < 1.00$, and lying almost precisely midway between the Eu^{2+} and Eu^{3+} lines, leading us to identify it as being due to intermediate-valence europium: $Eu^{2.5+}$. In many other intermediate-valence europium compounds such as $EuCu_2Si_2$ [10,11] and $EuPd_2Si_2$ [12], where the electron exchange is between the europium and the conduction band [13,14], the isomer shift of the intermediate-valence component is strongly temperature dependent [10] as electrons initially associated with the Eu^{2+} ions spend more time in the conduction band so that the average europium valence (and hence isomer shift) changes. That is not the case here and the electron exchange appears to be between the Eu^{2+} and Eu^{3+} ions. As long as the residence time on each ion is roughly the same, the time-averaged valence is constant, even if the residence time changes.

The area of the intermediate-valence feature is strongly dependent on both temperature and composition (Fig. 14). At base temperature, the area of the intermediate-valence feature is zero, but as temperature increases beyond T_{onset}, it starts to increase, with T_{onset} decreasing with increasing x, i.e., increasing with increasing Eu concentration. Figure 15 plots T_{onset} vs x; the extrapolation of the data to $x = 0$, i.e., pure $EuPd_3S_4$, suggests that T_{onset} should occur near 340 K and, as will be mentioned below, is indeed the temperature of a structural phase transition associated with valence ordering on the Eu site [15]. The inset to Fig. 15 shows the intermediate-valence area data presented in Fig. 14, plotted versus effective temperature, T/T_{onset}. The data scale well and this suggests that temperatures well above 340 K will need to be measured for pure $EuPd_3S_4$ in order to see the intermediate-valence signal. The progressive decrease in T_{onset} apparent in Fig. 15 for the La-substituted series suggests that lanthanum substitution reduces the barrier for valence fluctuations in $La_xEu_{1-x}Pd_3S_4$.

Finally, although the position of the $Eu^{2.5+}$ line appears to be both composition and temperature independent, its width is not. As is clear from Fig. 16, the $Eu^{2.5+}$ line becomes progressively sharper with increasing temperature, while the widths of the Eu^{2+} and Eu^{3+} lines remain unchanged. This sharpening is characteristic of motional narrowing. If the residence time of the electron is much longer than the characteristic measuring time used to detect the valence (∼10–100 ns for Mössbauer spectroscopy), then the system appears static and

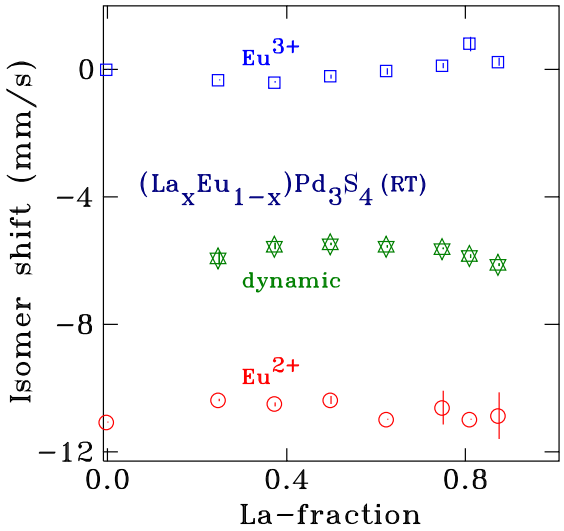

FIG. 13. Isomer shifts of the three components seen in the RT ^{151}Eu Mössbauer spectra of $La_xEu_{1-x}Pd_3S_4$ (shown in Fig. 12) showing that the values are relatively constant for all three, and that the dynamic, intermediate-valence component lies between the Eu^{2+} and Eu^{3+} component, suggesting a composition-independent valence of $\sim Eu^{2.5+}$.

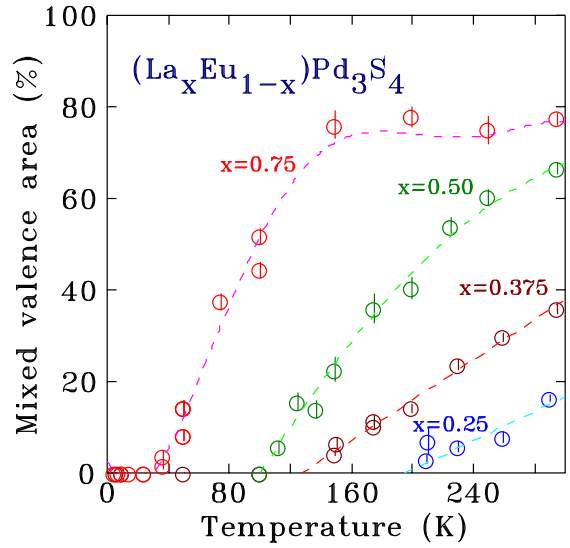

FIG. 14. Temperature dependence of the fitted area of the intermediate-valence feature for $La_xEu_{1-x}Pd_3S_4$ showing both the greater extent and earlier onset associated with increasing lanthanum substitution. Dashed lines are guides to the eye.

two distinct valence states are seen. If the residence time is much shorter, then an averaged valence is seen. Intermediate residence times ("slow relaxation") can lead to more complex behavior in the spectrum, but in the current case where the two components are single lines with no significant quadrupole or magnetic splittings, slow relaxation simply leads to a broad dynamic component. Raising the temperature generally leads to shorter residence times and the system evolves from fully static, through the slow relaxation regime, to dynamically averaged (or motionally narrowed). As can be seen by comparing Figs. 14 and 16 for $x = 0.75$, a weak broad line first appears near 80 K. On warming, it becomes stronger as more europium sites become dynamic, and sharper as the dynamics become faster and motional narrowing occurs. Finally, it develops into a natural-width line as the fluctuation rate increases and moves up, out of the Mössbauer window.

It is likely that the Eu^{2+}/Eu^{3+} dynamics and the development of intermediate-valence europium are the cause of the difference between the estimate of percentage of Eu^{2+} between the Mössbauer, $M(H)$, and $M(T)$ data for the lanthanum substituted samples shown in Fig. 6. The ^{151}Eu Mössbauer and the saturation magnetization measurements were made at 10 K and 1.8 K, respectively, well below T_{onset}, and the valence ratios derived from them are in agreement. However, the Curie-Weiss analysis relies on measurements made at much higher temperature ranges where the intermediate-valence behavior is both pronounced and temperature dependent. Indeed, as the intermediate-valence fraction becomes larger (Fig. 14), the Curie-Weiss-derived Eu^{2+} fraction deviates more strongly from the Mössbauer and saturation magnetization values (Fig. 6). A simple Curie-Weiss analysis of temperature-dependent susceptibility is not valid where the valence and hence europium moment is strongly temperature dependent.

Finally, we note that if the same intermediate-valence behavior is present in $Y_xEu_{1-x}Pd_3S_4$ at RT, it accounts for less than 10% of the total area (Fig. 11). The difference between the yttrium- and lanthanum-substituted series may reflect stabilization of Eu^{2+} by yttrium substitution, but there is also a very rapid loss of Eu^{3+} as yttrium is added, so as we approach the substitution levels where the $Eu^{2.5+}$ component dominated in $La_xEu_{1-x}Pd_3S_4$, there is almost no Eu^{3+} left in $Y_xEu_{1-x}Pd_3S_4$ to exchange electrons with the majority Eu^{2+},

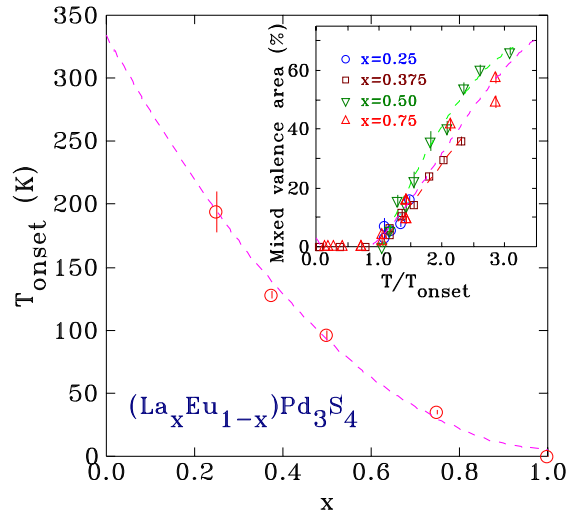

FIG. 15. Composition dependence of the temperature at which the intermediate-valence feature first appears in the ^{151}Eu Mössbauer spectra of $La_xEu_{1-x}Pd_3S_4$ (see Fig. 14). The dashed line is a guide to the eye showing an extrapolation to $x = 0$ that suggests a similar transition for pure $EuPd_3S_4$ near 340 K. The inset shows how the composition and temperature dependences from Fig. 14 collapse when scaled to T_{onset}.

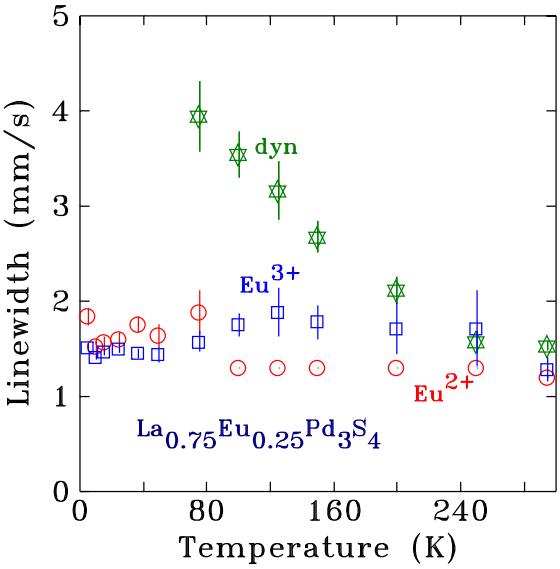

FIG. 16. Temperature dependence of the spectral linewidths for the three components seen in the ^{151}Eu Mössbauer spectra of $La_{0.75}Eu_{0.25}Pd_3S_4$. The Eu^{2+} and Eu^{3+} features have constant linewidths, as expected. However, the dynamic feature associated with the appearance of the $Eu^{2.5+}$ component clearly sharpens with increasing temperature, reflecting motional narrowing associated with an increasing relaxation rate.

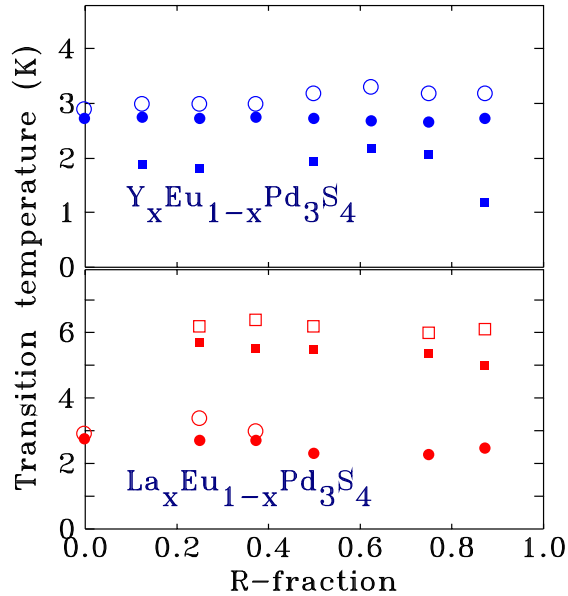

FIG. 17. Estimated transition temperatures for $Y_xEu_{1-x}Pd_3S_4$ (top) and $La_x00Eu_{1-x}Pd_3S_4$ (bottom). Open symbols show estimates derived from dc susceptibility, while solid symbols are based on C_p data.

so the absence of intermediate-valence europium may simply be the result of limited supply.

D. Magnetic ordering

Although the Eu^{2+} fraction does increase as yttrium is added, there is a steady decline in the net moment-bearing rare-earth content of the $Y_xEu_{1-x}Pd_3S_4$ series with increasing x. This decline is even stronger in the $La_xEu_{1-x}Pd_3S_4$ series as the Eu^{2+} fraction is either constant (up to $x \sim 0.5$) or decreases with increasing x. Despite these monotonic reductions in the moment-bearing fraction, Fig. 17 shows that both series continue to exhibit some form of magnetic order, at least as far as $x = 0.875$. Furthermore, it is apparent from both the high-field magnetization curves (Figs. 8 and 10) and low-field dc susceptibility (Figs. 20 and 22 in the Appendix) that both series develop some ferromagnetic character to their ordering. Heat-capacity measurements (Figs. 19 and 21 in the Appendix) confirm the persistence of magnetic ordering. With increasing dilution, the signature of the ordering becomes progressively weaker, with a softer onset, but it is never lost.

For $Y_xEu_{1-x}Pd_3S_4$, the onset of magnetic order appears to be largely insensitive to the level of substitution, remaining near 3 K for all x. However, the Y-substituted samples also exhibit a secondary feature around 2 K in the heat-capacity data, and it too is largely independent of the composition.

For $La_xEu_{1-x}Pd_3S_4$, the heat-capacity (Fig. 21 in the Appendix) and dc susceptibility (Fig. 22 in the Appendix) measurements show that the ordering behavior is more complex in the lanthanum-substituted series. Whereas the ~3 K feature from the parent compound persists for all finite x, but becomes progressively less distinct, a new feature develops at ~6 K as lanthanum is added. This is despite the steady dilution of the moment bearing component: by $x = 0.875$, only ~4% of the rare-earth atoms are moment-bearing Eu^{2+}, yet the 6 K magnetic feature is still apparent in both heat capacity and susceptibility. ^{151}Eu Mössbauer spectroscopy confirms that the 6 K feature at $x = 0.75$ is indeed magnetic and associated with the Eu^{2+} in the material. Although the ~5 K limit of the closed-cycle fridge was not low enough to yield a fully resolved magnetic splitting, Fig. 23 (in the Appendix) shows that it is possible to observe the initial line broadening that occurs as order develops. Fitting the broad Eu^{2+} line at 5.3 K yields a hyperfine field of 11(1) T. Figure 17 summarizes the composition dependence of the transition temperatures observed for $(Y, La)_xEu_{1-x}Pd_3S_4$.

The form of C_p (T) for $La_{0.25}Eu_{0.75}Pd_3S_4$, and to a lesser extent $La_{0.375}Eu_{0.625}Pd_3S_4$, might lead one to suspect that either an impurity phase is present or the sample has perhaps separated into La-rich and La-poor regions, yielding distinct ~6 K and ~3 K transitions, respectively. The magnitude of the C_p signal would require a rather significant impurity content to account for it. None was detected by x-ray diffraction, as noted earlier. Furthermore, the change in lattice parameter with x in the La-substituted series is quite strong (see Fig. 6), so any phase separation would yield broadened, or more likely split, diffraction lines. These were not seen in any sample studied here. Finally, the $NaPt_3O_4$ form of RPd_3S_4 appears to be stable across the entire rare-earth series and for both the Y- and La-substituted series studied here, giving us no reason to expect phase separation. The monotonic composition and temperature evolution of the intermediate-valence component apparent in Figs. 12 and 14 also argues for homogeneous rather than phase-separated samples. The ^{151}Eu Mössbauer spectra in Fig. 24 (in the Appendix) reveal a progressive development of magnetic order on cooling: The Eu^{2+} component near −11 mm/s first broadens below 6 K, then a full magnetic

pattern appears (more apparent on the low-velocity side of the Eu^{2+} component) on further cooling. Even at 1.8 K, the magnetic component is extremely broad (compare the 1.8 K spectrum in Fig. 24 (in the Appendix) with that of $EuPd_3S_4$ at the same temperature in Fig. 2). A simple parametrization of the spectra was obtained by using three components to fit the Eu^{2+} contribution: zero field, low field, and high field. Fewer components gave a poor fit, while using more led to instabilities. Following the areas of the magnetic and nonmagnetic Eu^{2+} components (Fig. 25 in the Appendix) shows a gradual shift from nonmagnetic to magnetic starting below 6 K with no apparent break near 3 K. The average magnetic field shown in Fig. 26 (in the Appendix) shows similar behavior, again with no break near 3 K. We conclude that although the Eu^{2+} experiences a very broad range of magnetic environments, there is no evidence for phase separation.

IV. DISCUSSION

Given that the RPd_3S_4 compound series exists for most, if not all, of the trivalent rare earths (R) and yttrium [1–4], but not, apparently, for the divalent alkaline earths, it is remarkable that $EuPd_3S_4$ not only accommodates such a large fraction of divalent europium, but that the fraction of Eu^{2+} is so robust against substitution by other trivalent rare earths: Substituting yttrium actually promotes the divalent state, whereas substituting lanthanum has little impact on the europium valence until at least half of the europium has been replaced.

It is clear that band filling or average valence electron count does not control the Eu^{2+}:Eu^{3+} ratio in $R_xEu_{1-x}Pd_3S_4$ as both yttrium and lanthanum are trivalent yet act on the Eu^{2+}:Eu^{3+} ratio in opposite directions. Similarly, chemical pressure arguments fail as lattice compression using yttrium substitution favors the larger Eu^{2+} ion, and lattice expansion using lanthanum leads to more of the smaller Eu^{3+} ion—the reverse of what would be predicted.

We are left with preservation of the average rare-earth size as the dominant factor controlling the Eu^{2+}:Eu^{3+} valence ratio. Since $r_{\mathrm{ionic}}(Y^{3+})$ is both smaller than $r_{\mathrm{ionic}}(Eu^{3+})$ and much smaller than $r_{\mathrm{ionic}}(Eu^{2+})$, converting Eu^{3+} into the larger Eu^{2+} as yttrium is added acts to maintain the average rare-earth size. By the same token, $r_{\mathrm{ionic}}(La^{3+})$ lies between those of Eu^{2+} and Eu^{3+}, so lanthanum substitution initially has very little effect on the Eu^{2+}:Eu^{3+} ratio. Only after half of the europium has been replaced do we see a shift in the balance towards Eu^{3+}.

Hydrostatic pressure would provide a complementary window on how pure changes in volume affect the Eu^{2+}:Eu^{3+} ratio, and synchrotron Mössbauer spectroscopy under pressure would be a useful extension of this study.

Remarkably, La substitution also appears to reduce the barrier for valence fluctuations between the Eu^{2+} and Eu^{3+} in $La_xEu_{1-x}Pd_3S_4$, and a temperature-dependent intermediate-valence component develops at progressively lower temperatures with increasing lanthanum content. Extrapolating the composition trend in the onset temperature leads to the prediction that valence fluctuations should start around 340 K in undoped $EuPd_3S_4$. The much weaker dynamic behavior in the Y-substituted series may reflect a stronger bias towards Eu^{2+} in $Y_xEu_{1-x}Pd_3S_4$, which may in turn stabilize the valence of the two europium components. Alternatively, the much lower availability of Eu^{3+} for electron exchange may be the limiting factor.

The evolution of low-temperature magnetism, as seen by Mössbauer spectroscopy, heat capacity, and low-field magnetic susceptibility also differs between yttrium and lanthanum. Remarkably, suppression of the ordering by the dilution of the magnetic Eu^{2+} is not the primary impact in either series. Magnetic order persists in $Y_xEu_{1-x}Pd_3S_4$ even as far as $x = 0.875$, with the onset temperature essentially unchanged, despite only about 12% of the europium sites being occupied by a moment-bearing ion (Fig. 17). However, the behavior of the La-substituted series is perhaps more surprising. Not only does the magnetic order also persist to $x = 0.875$ (where the moment-bearing fraction is only ∼4% because of the much lower Eu^{2+}:Eu^{3+} ratio in the La-substituted series), but the onset temperature jumps from ∼3 K to ∼6 K for low x and remains near 6 K at least as far as $x = 0.875$ (Fig. 17). We emphasize that our data do not provide access to the specific magnetic structures of the Y- and La-substituted materials. The behavior of χ (T) and C_p (T) in Fig. 5 strongly suggests that the parent compound orders antiferromagnetically; however, it is unlikely that this survives the substitutional disorder introduced when we replace the europium. The form of χ (T) clearly changes in both series (Figs. 20 and 22 in the Appendix) and the magnetic order appears to develop at least some ferromagnetic character, although it is probably dominated by short-range order. The extremely broad hyperfine field distributions and the presence of significant zero-field components well below the onset of magnetic order in both $La_{0.25}Eu_{0.75}Pd_3S_4$ and $Y_{0.25}Eu_{0.75}Pd_3S_4$ (Fig. 27) point to inhomogeneous ordering in both of these magnetically diluted materials.

Finally, we need to address the question of whether $EuPd_3S_4$ is a heterogeneous or randomly arranged mixed-valence system, as has been generally assumed, or is actually valence ordered. Many observations, both by us and others, point indirectly to the latter possibility as more likely. The sharp heat-capacity susceptibility cusps seen here (Fig. 19) and by Wakeshima *et al.* [5] in $EuPd_3S_4$ and by Matsuoka *et al.* [16] in $YbPd_3S_4$, taken with the long-range-ordered AF structure seen by neutron diffraction in $YbPd_3S_4$ [16] and, more recently, in $EuPd_3S_4$ [15], all point to a spatially ordered Eu^{2+} lattice. Similarly, residual resistance ratios (RRRs) of ∼15 ($EuPd_3S_4$) and ∼9 ($YbPd_3S_4$) in sintered materials [17], and as much as 40 in flux-grown single crystals of $EuPd_3S_4$ [18,19], are also more consistent with an ordered valence structure. However, the response to doping provides perhaps the strongest evidence that the parent $EuPd_3S_4$ is valence ordered. Figures 19–22 show that even modest substitutions by yttrium or lanthanum have profound effects on the magnetic order, far beyond anything that might be attributable to simple dilution. Local measurements using ^{151}Eu Mössbauer spectroscopy tell a similar story: contrast the sharp magnetic pattern in $EuPd_3S_4$ with the severely broadened spectra in the lanthanum- and yttrium-substituted materials at 1.8 K (Fig. 27). The many differences between the definitely disordered $Y_xEu_{1-x}Pd_3S_4$ and $La_xEu_{1-x}Pd_3S_4$, on the one hand, and the possibly ordered $EuPd_3S_4$ on the other, are sufficiently

striking that we are forced to suggest that $EuPd_3S_4$ is, in fact, valence ordered with a 50:50 mix of Eu^{2+} and Eu^{3+} ions.

Direct confirmation of valence ordering has been provided recently by single-crystal x-ray diffraction measurements that have shown that the correct crystal structure for $EuPd_3S_4$, at and below ambient temperatures, is the slightly lower symmetry $Pm\bar{3}$ (No. 200) [15]. The $2a$ Eu site in the $Pm\bar{3}n$ cell is split into a $1a$ at (000) and a $1b$ at $(\frac{1}{2}\frac{1}{2}\frac{1}{2})$, with the $1a$ being slightly larger to accommodate the larger Eu^{2+} ion. The Pd and S atoms are displaced by ~1% from their special positions in the $Pm\bar{3}n$ cell. The lowered symmetry releases the $hhl,\ l = 2n$, and $h00,\ h = 2n$ constraints so that the (100) and (111) reflections are allowed. However, they are extremely weak (~0.1% of the strongest reflections) and we were unable to observe them in our powder diffraction data. The ordered structure appears to revert to the disordered $Pm\bar{3}n$ form near 340 K [15], consistent with our extrapolated T_{onset} shown in Fig. 15.

V. CONCLUSIONS

The impact of yttrium and lanthanum substitution on mixed-valence $EuPd_3S_4$ has been studied using ^{151}Eu Mössbauer spectroscopy, bulk magnetization, and heat-capacity measurements. Average valence electron count clearly does not control the europium valence distribution as trivalent yttrium and lanthanum substitutions have opposite effects. Similarly, chemical pressure arguments fail, as lattice compression using yttrium substitution favors the larger Eu^{2+} ion, with the reverse effect seen with lanthanum. It appears that preservation of the average rare-earth size is the dominant factor controlling the Eu^{2+}:Eu^{3+} valence ratio.

Lanthanum substitution was also found to promote valence instability between the Eu^{2+} and Eu^{3+} ions, leading to the formation of intermediate-valence europium. Increasing lanthanum substitution both increases the amount of intermediate-valence europium seen at ambient temperatures and reduces the temperature at which fluctuations start to appear. An onset temperature of ~340 K is predicted for undoped $EuPd_3S_4$.

Inhomogeneous magnetic order is seen at all levels of substitution, with the onset temperature in the Y-substituted series being essentially unchanged at 3 K, while for the La-substituted series, the onset temperature is seen to increase to 6 K despite the low concentration of magnetic ions.

Many of our observations suggest that the parent compound, $EuPd_3S_4$, is valence ordered, and this has recently been confirmed by single-crystal x-ray diffraction data [15].

ACKNOWLEDGMENTS

Financial support for this work was provided by Fonds Québécois de la Recherche sur la Nature et les Technologies, and the Natural Sciences and Engineering Research Council (NSERC) Canada. Work at the Ames Laboratory was supported by the U.S. Department of Energy, Office of Science, Basic Energy Sciences, Materials Sciences and Engineering Division. The Ames Laboratory is operated for the U.S. Department of Energy by Iowa State University under Contract No. DE-AC02-07CH11358. B.K. is supported by the Center for the Advancement of Topological Semimetals (CATS), an Energy Frontier Research Center funded by the U.S. DOE, Office of Basic Energy Sciences. Much of this work was carried out while D.H.R. was on sabbatical at Iowa State University and their generous support during this visit is gratefully acknowledged.

APPENDIX: ADDITIONAL FIGURES AND TABLES

This Appendix contains additional figures showing the crystallographic structure of the parent $EuPd_3S_4$ along with heat-capacity and susceptibility data for $Y_xEu_{1-x}Pd_3S_4$ and $La_xEu_{1-x}Pd_3S_4$.

We also present low-temperature ^{151}Eu Mössbauer data for $La_{0.5}Eu_{0.5}Pd_3S_4$ showing the onset of magnetic broadening near 6 K, and spectra for $La_{0.25}Eu_{0.75}Pd_3S_4$ showing the inhomogeneous magnetic order that develops below the transition temperature. The temperature dependence of some fitting parameters for the $La_{0.25}Eu_{0.75}Pd_3S_4$ spectra is also shown.

The fitted lattice parameters and Eu^{2+} fractions used to construct Fig. 6 in the main body of the text are also tabulated here.

TABLE I. Measured lattice parameters and Eu^{2+} fractions for the $Y_xEu_{1-x}Pd_3S_4$ compound series.

		Eu^{2+} fraction (%)		
x	a (Å)	Mössbauer	Curie-Weiss ±5%	$M(H)$ ±5%
0.00	6.67858(8)	53.8(5)	57	49
0.125	6.67637(9)	56.3(8)	59	56
0.25	6.67371(13)	61.5(5)	66	63
0.375	6.66983(12)	68.4(5)	72	68
0.500	6.66527(20)	73.3(9)	71	69
0.625	6.66148(10)	83.2(7)	92	89
0.750	6.65514(12)	87.3(8)	85	86
0.875	6.64921(11)	93(2)	95	94
1.00	6.64193(17)			

TABLE II. Measured lattice parameters and Eu^{2+} fractions for the $La_xEu_{1-x}Pd_3S_4$ compound series.

		Eu^{2+} fraction (%)		
x	a (Å)	Mössbauer	Curie-Weiss ±5%	$M(H)$ ±5%
0.00	6.67858(8)	53.8(5)	57	49
0.25	6.69217(18)	53.1(6)	55	52
0.375	6.70125(17)	51.1(9)	53	49
0.50	6.70871(17)	51.5(8)	54	49
0.625	6.71763(12)	47(2)	53	46
0.75	6.72490(14)	46(2)	56	43
0.8125	6.72981(12)	39(1)	57	40
0.875	6.73316(14)	32(1)	61	36
0.9375	6.73557(6)	25(3)	86	34
1.00	6.73948(9)			

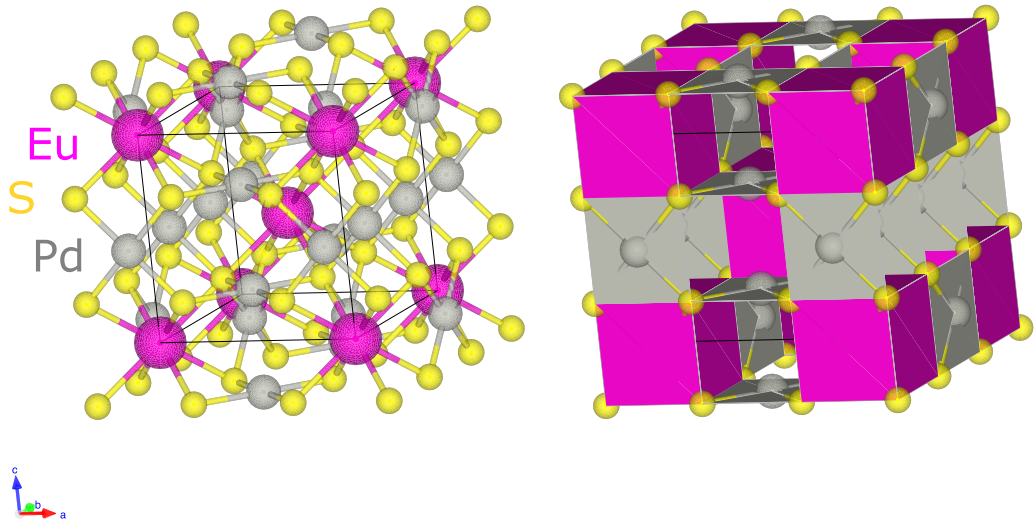

FIG. 18. The cubic $NaPt_3O_4$ structure ($Pm\bar{3}n$ No. 223) adopted by $EuPd_3S_4$. The left-hand panel shows a ball and stick model emphasizing the first-neighbor bonding around each atom. The right-hand panel shows the coordination polyhedra with the europium atoms on the $2a$ sites eightfold coordinated by a cubic arrangement of sulphur atoms. The atoms are shown as Eu (magenta), Pd (gray), and S (yellow). Note that the small distortions leading to the lower-symmetry $Pm\bar{3}$ structure [15] cannot be seen on this scale. Figures are drawn using VESTA [20].

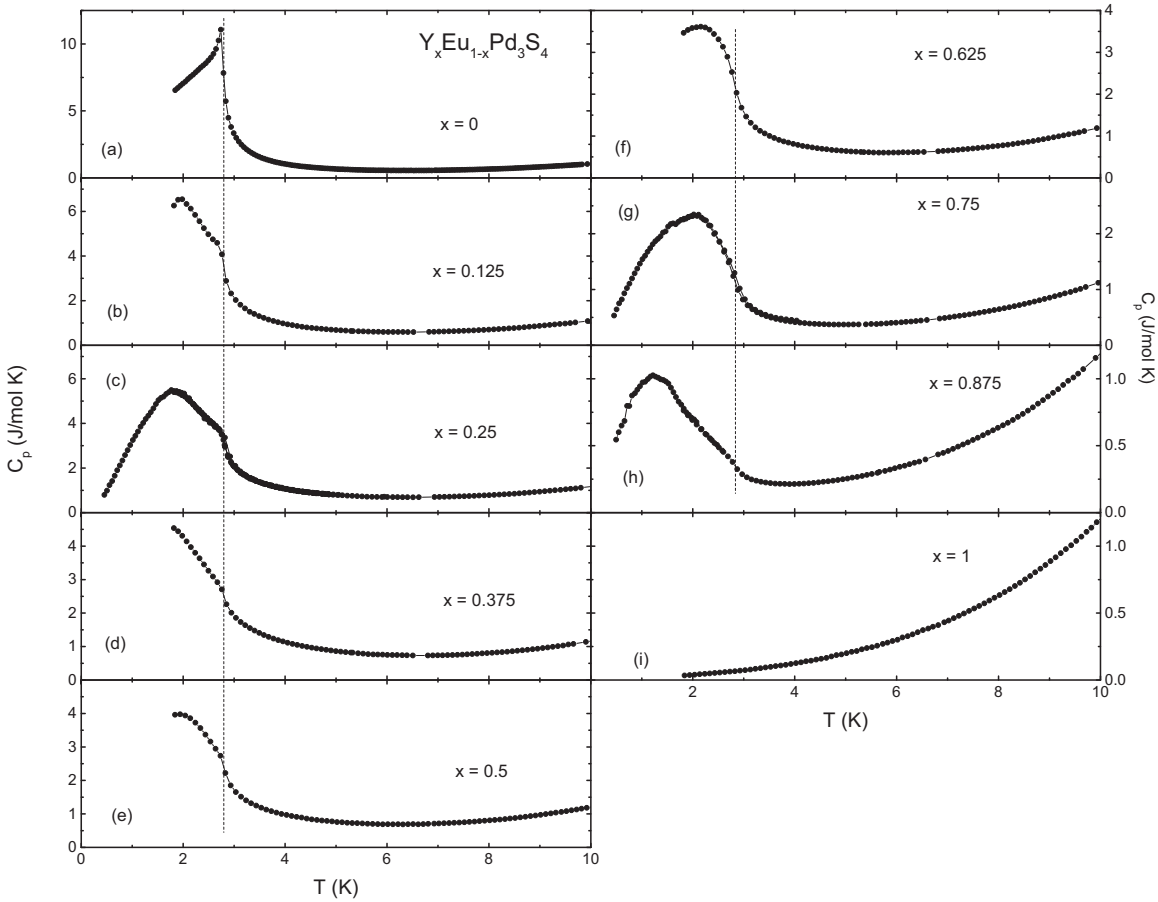

FIG. 19. Heat-capacity measurements for $Y_xEu_{1-x}Pd_3S_4$ showing the persistence of the magnetic transition near 3 K despite the significant dilution of the magnetic Eu^{2+}. At $x = 1$, there is no transition observed as the system contains no magnetic species and so is paramagnetic. The vertical dashed lines mark 3 K.

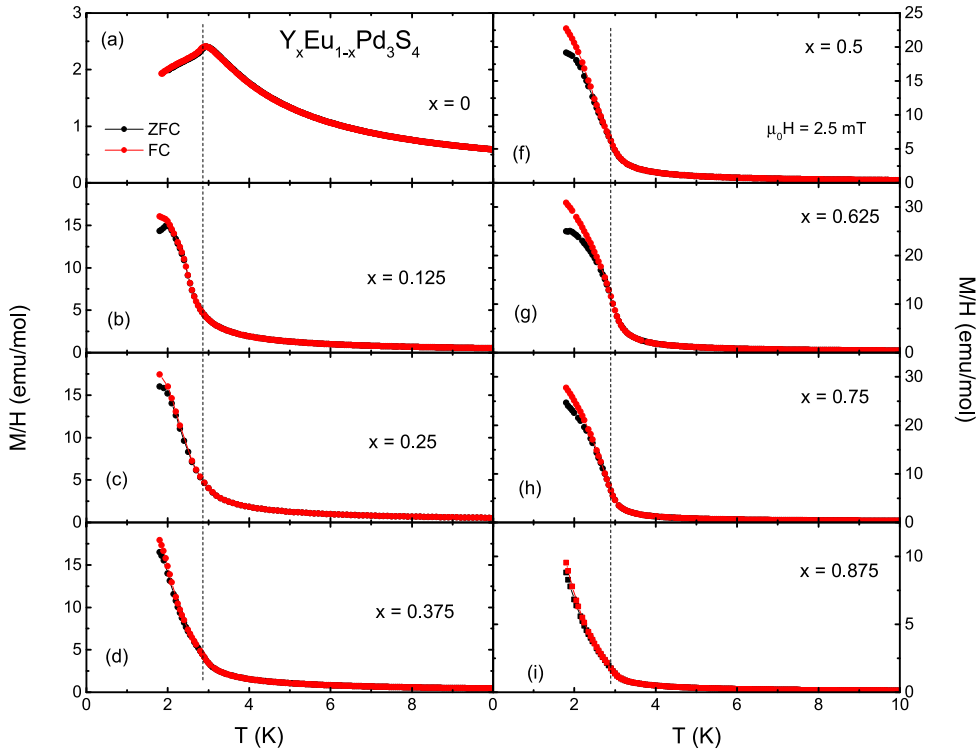

FIG. 20. Field-cooled (FC) and zero-field-cooled (ZFC) dc susceptibility for $Y_xEu_{1-x}Pd_3S_4$ confirming the persistence of the magnetic transition seen near 3 K in the heat-capacity data (Fig. 19) despite the significant dilution of the magnetic Eu^{2+}. The vertical dashed lines mark 3 K.

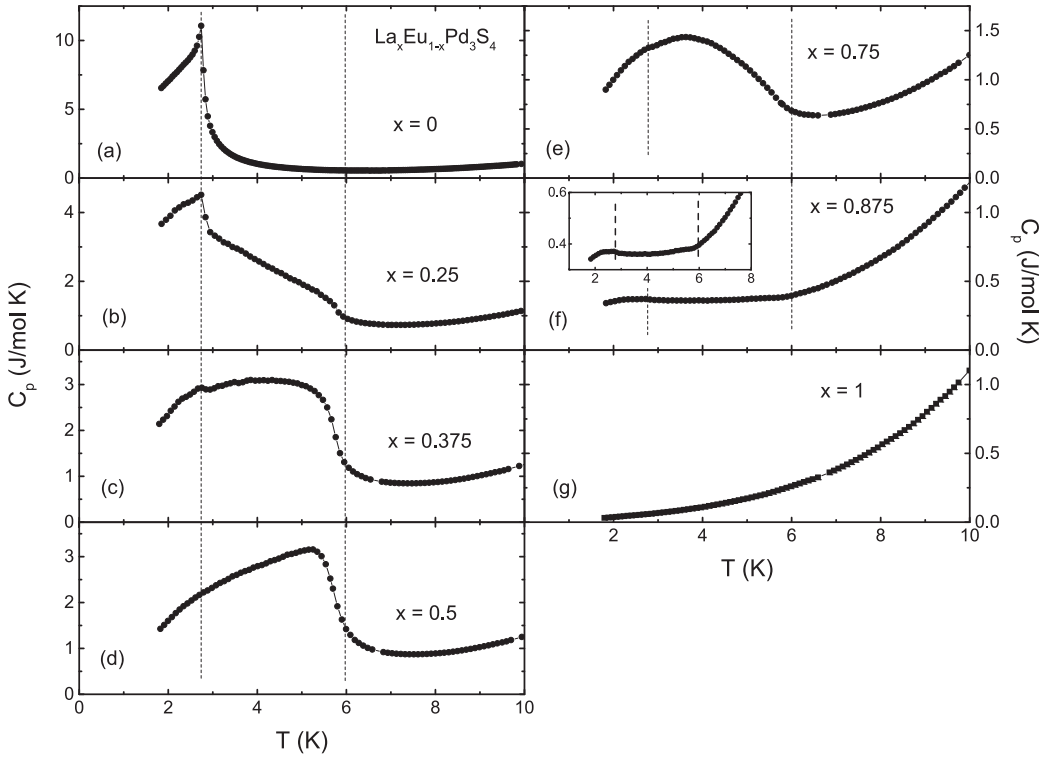

FIG. 21. Heat-capacity measurements for $La_xEu_{1-x}Pd_3S_4$ showing the gradual replacement of the 3 K transition by a new feature at 6 K, despite the significant dilution of the magnetic Eu^{2+} component. The inset in (f) shows the region between 2 K and 8 K on an expanded vertical scale. At $x = 1$, there is no transition observed as the system contains no magnetic species and so is paramagnetic. The vertical dashed lines mark 3 K and 6 K.

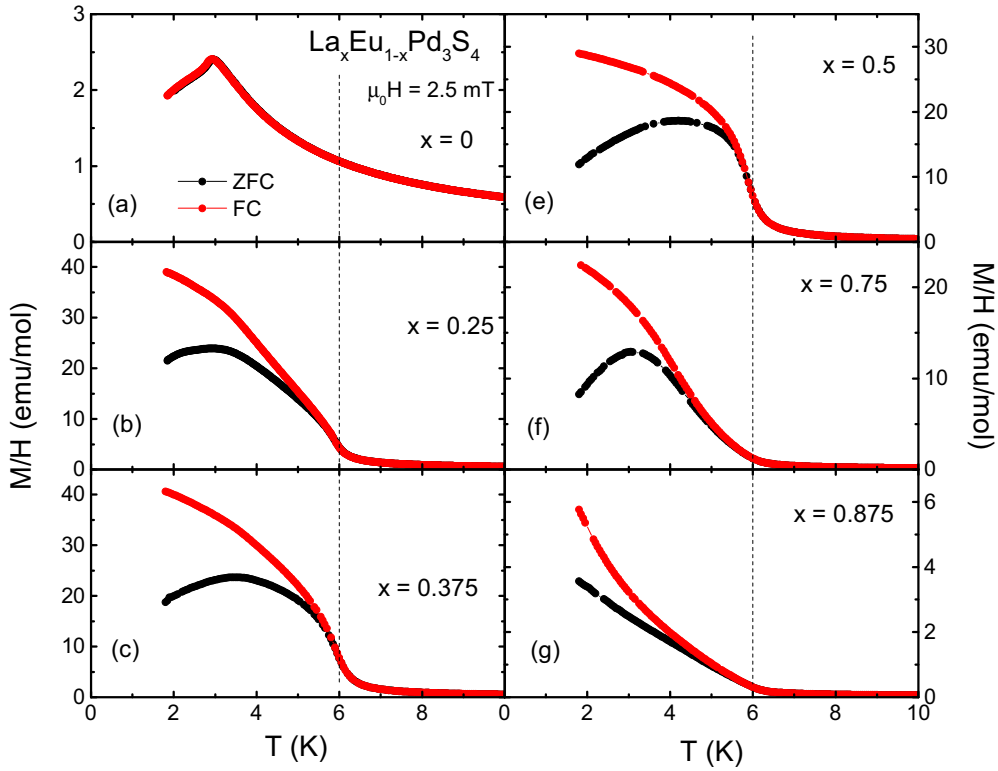

FIG. 22. Field-cooled (FC) and zero-field-cooled (ZFC) dc susceptibility for $La_xEu_{1-x}Pd_3S_4$ confirming the gradual replacement of the 3 K transition by a new feature at 6 K, seen in the heat-capacity data (Fig. 21) despite the significant dilution of the magnetic Eu^{2+}. The vertical dashed lines mark 6 K.

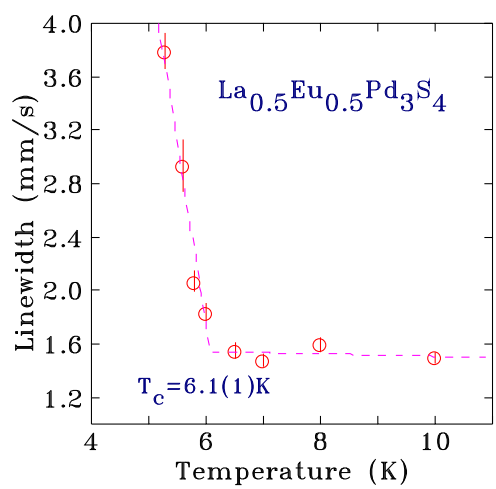

FIG. 23. Temperature dependence of the Eu^{2+} line width in $La_{0.5}Eu_{0.5}Pd_3S_4$ showing the onset of ordering at 6.1(1) K.

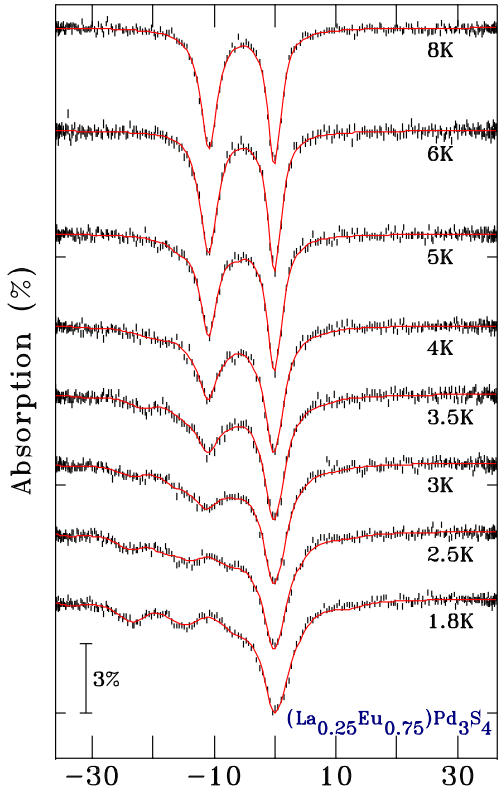

FIG. 24. ^{151}Eu Mössbauer spectra of $La_{0.25}Eu_{0.75}Pd_3S_4$ showing the progressive development of magnetic order in the Eu^{2+} component. The solid lines are fits using a single line for the Eu^{3+} line near 0 mm/s, and three components to fit the Eu^{2+}: an unsplit line, and two magnetic contributions with a "small" and "large" field used to reproduce the gross behavior of the system.

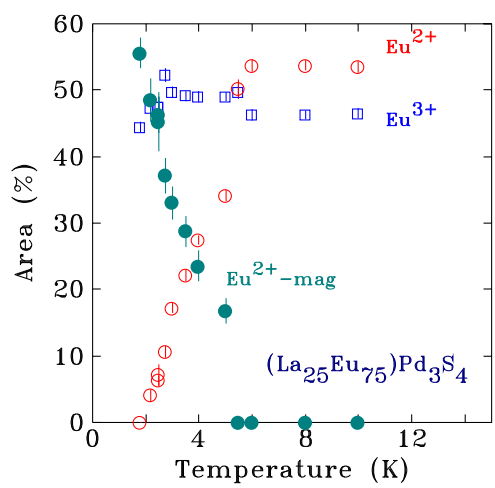

FIG. 25. Temperature dependence of the magnetic and nonmagnetic Eu^{2+} components in the ^{151}Eu Mössbauer spectra of $La_{0.25}Eu_{0.75}Pd_3S_4$ showing the gradual onset of magnetic order below 6 K, but no evidence for a break at 3 K that might suggest the presence of a second phase.

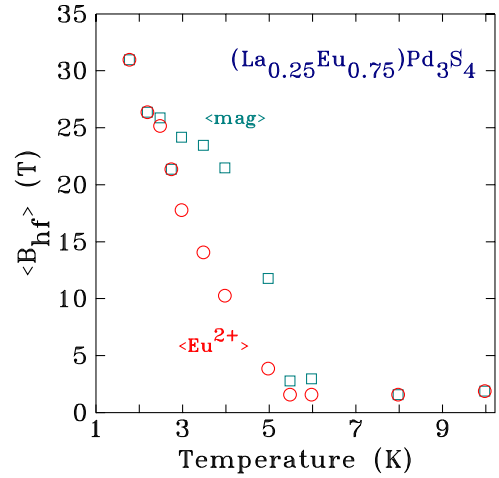

FIG. 26. Temperature dependence of the average Eu^{2+} magnetic hyperfine field (B_{hf}) in the ^{151}Eu Mössbauer spectra of $La_{0.25}Eu_{0.75}Pd_3S_4$ showing the gradual onset of magnetic order below 6 K. Two averages are shown: (i) $\langle Eu^{2+}\rangle$ (blue circles) is calculated for all three Eu^{2+} components used in the fits; (ii) $\langle$mag$\rangle$ (red squares) is calculated omitting the Eu^{2+} component that exhibits no magnetic splitting. See text for details of the model used to fit the spectra.

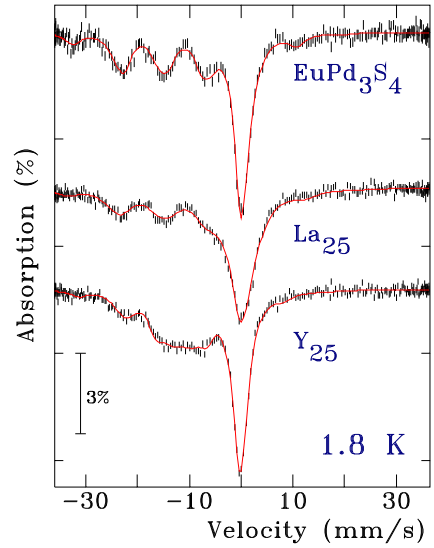

FIG. 27. ^{151}Eu Mössbauer spectra of $EuPd_3S_4$ (top), $La_{0.25}Eu_{0.75}Pd_3S_4$ (middle), and $Y_{0.25}Eu_{0.75}Pd_3S_4$ (bottom) measured at 1.8 K showing that while the substituted materials do appear to exhibit magnetic ordering of the Eu^{2+} component, the lines are not sharp, reflecting a broad distribution of hyperfine fields.

[1] D. A. Keszler, J. A. Ibers, and M. H. Mueller, J. Chem. Soc., Dalton Trans., 2369 (1985).
[2] M. Wakeshima, T. Fujino, N. Sato, K. Yamada, and H. Masuda, J. Solid State Chem. **129**, 1 (1997).
[3] M. Wakeshima and Y. Hinatsu, J. Solid State Chem. **146**, 226 (1999).
[4] P. Bonville, C. Godart, E. Alleno, F. Takahashi, E. Matsuoka, and M. Ishikawa, J. Phys.: Condens. Matter **15**, L263 (2003).
[5] M. Wakeshima, Y. Doi, Y. Hinatsu, and N. Masaki, J. Solid State Chem. **157**, 117 (2001).
[6] A. C. Larson and R. B. Von Dreele, General structure analysis system, Report No. LAUR 86-748, Los Alamos National Laboratory (2000).
[7] B. H. Toby, J. Appl. Crystallogr. **34**, 210 (2001).
[8] C. J. Voyer and D. H. Ryan, Hyperfine Interact. **170**, 91 (2006).
[9] K. Abe, J. Kitagawa, N. Takeda, and M. Ishikawa, Phys. Rev. Lett. **83**, 5366 (1999).
[10] E. R. Bauminger, D. Froindlich, I. Nowik, S. Ofer, I. Felner, and I. Mayer, Phys. Rev. Lett. **30**, 1053 (1973).
[11] A. Palenzona, S. Cirafici, and F. Canepa, J. Less-Common Met. **119**, 199 (1986).
[12] M. M. Abd-Elmeguid, C. Sauer, and W. Zinn, J. Phys. C: Solid State Phys. **18**, 345 (1985).
[13] J. Röhler, D. Wohlleben, G. Kaindl, and H. Balster, Phys. Rev. Lett. **49**, 65 (1982).
[14] Z. Hossain, C. Geibel, N. Senthilkumaran, M. Deppe, M. Baenitz, F. Schiller, and S. L. Molodtsov, Phys. Rev. B **69**, 014422 (2004).
[15] T. Berry *et al.* (unpublished).
[16] E. Matsuoka, F. Takahashi, J. Kitagawa, K. Ohoyama, H. Yoshizawa, and M. Isikawa, J. Magn. Magn. Mater. **231**, 23 (2001).
[17] J. Kitagawa, T. Takabatake, E. Matsuoka, F. Takahashi, K. Abe, and M. Ishikawa, J. Phys. Soc. Jpn. **71**, 1630 (2002).
[18] T. J. Slade and P. C. Canfield, Zeitschrift für anorganische und allgemeine Chemie **648**, e202200145 (2022).
[19] S. Huyan *et al.* (unpublished).
[20] K. Momma and F. Izumi, J. Appl. Crystallogr. **44**, 1272 (2011).